PRAMANA — journal of physics
© Indian Academy of Sciences
Vol. 80, No. 2
February 2013
pp. 315–326

Effect of Al doping on microstructure and optical band gap of ZnO thin film synthesized by successive ion layer adsorption and reaction

S MONDAL[1], S R BHATTACHARYYA[2] and P MITRA[1,*]

[1]Department of Physics, The University of Burdwan, Rajbati, Bardhaman 713 104, Burdwan, India
[2]Surface Physics Division, Saha Institute of Nuclear Physics, 1/AF Bidhan Nagar, Kolkata 700 064, India
*Corresponding author. E-mail: mitrapartha1@rediffmail.com

MS received 24 January 2012; accepted 22 August 2012

Abstract. Thin films of pure and aluminum-doped zinc oxide (AZO) were deposited on glass substrates from ammonium zincate bath following a chemical dipping technique called successive ion layer adsorption and reaction (SILAR). Characterization techniques such as X-ray diffraction (XRD), scanning electron microscopy (SEM) and energy-dispersive X-rays (EDX) were used to investigate the effect of Al doping on the microstructure of AZO films. Particle size analysis using X-ray line broadening shows marginally increasing trend with increasing Al impurity. The average particle size for pure ZnO is 22.75 nm. It increases to 24.26 nm for 1% AZO film and 25.13 nm for 2% AZO film. Incorporation of Al was confirmed from elemental analysis using EDX. SEM micrograph shows that pure ZnO particles are spherical shaped. However, AZO films show particles with off-spherical shape with compact interconnected grains. The value of band gap for pure ZnO is 3.229 eV and it increases to 3.29 eV for 1% AZO indicating a blue-shift for 1% AZO film. However, for 2% AZO film, a decrease in band gap compared to pure ZnO is observed indicating a red-shift of fundamental absorption edge. Electrical resistance shows an initial decrease with increasing Al content. With further enhancement of Al incorporation, the resistance increases.

Keywords. Successive ion layer absorption and reaction; Al:ZnO thin films; microstructure; particle size; scanning electron microscopy; optical band gap.

PACS Nos **68.55.−a; 78.20.−e; 81.15.−z; 78.66.Hf**

1. Introduction

Zinc oxide is one of the most prominent metal oxide semiconductors with a direct energy wide band gap around 3.2–3.37eV at 300 K [1,2]. It is an *n*-type semiconductor of hexagonal (wurtzite) structure. It demonstrates many outstanding characteristics due to its good

DOI: 10.1007/s12043-012-0463-6; ***e*****Publication: 23 January 2013**

optical quality, abundance in nature, non-toxicity, thermal and chemical stability, excellent piezoelectric and semiconducting properties [3]. Due to this versatility, ZnO has drawn considerable attention and has been investigated in various forms such as single crystals, sintered pellets, thick films, nanobelts and thin films [2,4–10]. Thin films of ZnO find a multitude of immensely important applications in electronic and optoelectronic devices such as transparent conductors, solar cell windows, gas sensors, surface acoustic wave (SAW) devices, heat mirrors etc. [4–6]. It is also being considered as a potential candidate in the new frontiers of research like spintronics [7].

The performance and efficiency of thin film-based devices are determined strongly by the structural, electrical and optical properties of the component films. A study of these properties and their dependence on the film characteristics is very important as it helps in optimizing film parameters for better device applications. Further, the electrical and optical properties of thin films are determined by the process parameters during film growth as well as by the presence of impurities and defects in the films. For transparent conducting oxide (TCO) thin films such as ZnO, it is always desirable to improve the electrical conduction without affecting its excellent optical properties. As such, it is very important to optimize the process parameters of film growth and doping levels for an enhanced device performance. Al is chosen as dopant material because of its abundance. Doping with Al is primarily done to achieve high transparency, stability, high conductivity and also, because it enhances the gas-sensing properties of the ZnO thin films, which have immensely important industrial and domestic applications for detecting hazardous gases, including LPG [10,11]. AZO films have got potential applications in solar cells, solid-state display devices, optical coatings, heaters, defrosters, chemical sensors etc. [12,13]. Accordingly, synthesis of polycrystalline aluminum-doped ZnO (AZO) thin films has been widely carried out using different techniques such as ultrasonic chemical vapour deposition [13], spray pyrolysis [2,14], pulsed laser deposition [15,16], RF magnetron sputtering [3,17–19], helicon-wave excited plasma (HWP) deposition [20], electroless deposition [21], sol–gel [22,23], pulsed laser ablation [24,25], chemical beam deposition [26] and successive ion layer absorption and reaction (SILAR) [27,28] etc.

The conventional physical techniques give uniform and compact films with high transparency. They are generally safe (no toxic gas emissions) and have deposition rate at room temperature. However, they are usually very expensive and are difficult to expand to large scale. Low-temperature chemical techniques involving aqueous route (from solutions) on the other hand, are versatile, simple and cost-effective compared to vapour-phase techniques. They are easy for upscaling to industrial applications. Among the various chemical techniques, one of the less used and less studied chemical techniques is the successive ionic layer adsorption and reaction (SILAR). The SILAR method, also known as the modified version of chemical bath deposition, has a number of advantages apart from it being inexpensive, simple and convenient for large-scale deposition. The basic building blocks in SILAR are ions instead of atoms and therefore the preparative parameters are easily controllable. In this technique a substrate is dipped alternately into beakers containing aqueous solutions or distilled water for the reaction to take place at the substrate surface. The substrate can be introduced into various reactants for a specific length of time depending on the nature and kinetics of the reaction. The immersion-reaction cycle can be repeated for any number of times, limited only by the inherent problems associated with the deposition technique and the substrate–thin film interface. The technique is

called SILAR since it involves adsorption of a layer of complex ion on the substrate followed by reaction of the adsorbed ion layer. Since the synthesis can be carried out under mild conditions and at lower processing temperatures, implantation of metal ions at low temperatures is particularly suitable by this method.

The present study deals with the preparation of aluminum-doped ZnO (AZO) thin films on glass substrates by SILAR method. Earlier, Rakhshani [27] reported the preparation of AZO films by SILAR using sodium zincate complex. We also reported preparation of AZO films by SILAR from sodium zincate complex [28]. However, use of sodium complex always introduces highly mobile sodium ions in the films [29], which can be detrimental for their practical applications. In the present work, ammonium zincate complex was used to eliminate the incorporation of highly mobile sodium ions in the films. The objective of this research includes detailed microstrucural characterization of the coated films. The films have been characterized by different techniques such as X-ray diffraction (XRD), scanning electron microscopy (SEM), optical absorption and electrical resistivity for further investigation, which is essential to make full use of their active properties.

2. Experimental method

Pure zinc oxide films were deposited on glass substrates (microscope slides) by alternatively dipping into 0.1 M ammonium zincate [$(NH_4)ZnO_2$] bath kept at room temperature and hot water maintained near the boiling point. The glass substrate was cleaned, before deposition, by chromic acid followed by distilled water rinse and ultrasonic cleaning with acetone and alcohol. The cleaned substrate was tightly held in a holder so that only a requisite area for film deposition was exposed. Thus, the area for film deposition could be easily varied by adjusting the holder arrangement.

The ammonium zincate bath, used for deposition, was prepared by adding ammonium hydroxide (∼25% pure ammonia solution; Merck, Mol. Wt. 17.03 g/mol, density 0.91) to an aqueous solution of zinc acetate dihydrate [$Zn(CH_3COO)_2 2H_2O$]. The pH of the zincate solution was 10.80. pH measurement was carried out in a systronics pH meter (Model 335). Aluminium doping was carried out by adding hexahydrate aluminium chloride ($AlCl_3 \cdot 6H_2O$, Merck) in ammonium zincate bath.

The details of pure ZnO film deposition process from ammonium or sodium zincate bath has been reported earlier [28,30,31]. Briefly, a precleaned substrate (microscopic glass slide) was alternatively dipped in zinc complex solution (sodium zincate or ammonium zincate bath) kept at room temperature and hot water bath maintained at ∼95–98°C. One set of dipping involves dipping in zincate bath for 2 s and dipping in hot water bath for 2 s. Fifty dippings were performed for this experiment. The aluminium concentration was varied upto 2% in the bath solution. All the deposited films were white and homogeneous. After deposition, the peel-off test was conducted to confirm the adhesivity of the coated films on glass substrates which showed that well adherent films were formed. The thickness of the films was measured by the weight difference-density consideration [30,32] method using an electronic high-precision balance. The thickness for pure ZnO film was ∼0.8 μm. Growth rate of the films was found to increase due to Al incorporation. The thickness of 1% Al-doped film was found to be ∼0.96 μm.

Phase identification and crystalline properties of the films were studied by XRD method employing a Philips PW 1830 X-ray diffractometer with CuK_{α} radiation ($\lambda = 1.5418$). The experimental peak positions were compared with the standard JCPDS files and the Miller indices were indexed to the peaks. Scanning electron microscopy (Model S530, Hitachi, Japan) was used to study the surface morphology and to illustrate the formation of crystallites on the film surface. UV–VIS spectrophotometric measurements were performed using a spectrophotometer (Shimadzu, UV-1800) at room temperature. The spectra were recorded using a similar glass as a reference and hence the absorption due to the film only was obtained. The band gap of the films has been calculated from the absorption edge of the spectrum.

3. Results and discussions

3.1 *Structural characterization*

The XRD spectra of pure ZnO film and ZnO films doped with different Al content are presented in figure 1. The films were annealed at 350°C for 2 h in air prior to structural characterization. The diffraction pattern for pure ZnO is shown in figure 1a. Figures 1b, 1c, 1d, 1e and 1f show diffractograms for 0.5% AZO, 0.75% AZO, 1% AZO, 1.5% AZO

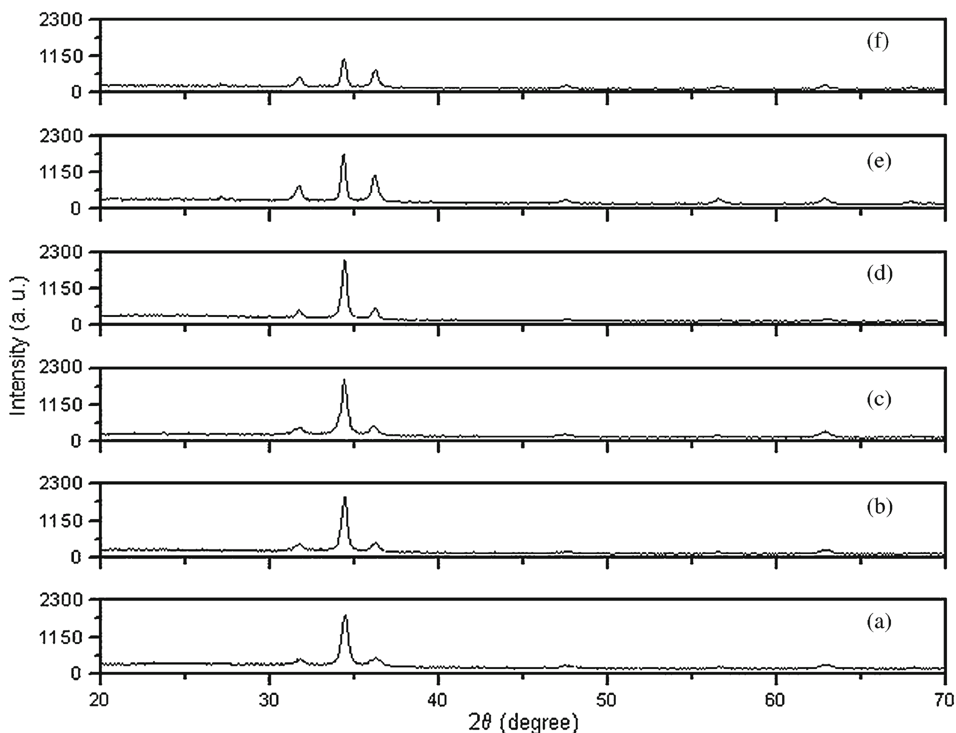

Figure 1. X-ray diffraction pattern of (**a**) ZnO, (**b**) 0.5% AZO, (**c**) 0.75% AZO, (**d**) 1% AZO, (**e**) 1.5% AZO and (**f**) 2% AZO.

and 2% AZO respectively. The diffraction angle 2θ was scanned in the range 20°–70°. The 2θ variation was employed with a 0.05° step and a time step of 1 s. Intensity in arbitrary units is plotted against 2θ in figure 1. It is seen from figure 1a that peaks appear at 31.75°, 34.389°, 36.205°, 47.434°, 56.576° and 62.855°. The diffractogram of the sample reveals that all the peaks are in good agreement with the joint committee on powder diffraction standard (JCPDS) data belonging to hexagonal ZnO structure [33]. The corresponding reflecting planes are (1 0 0), (0 0 2), (1 0 1), (1 0 2), (1 1 0) and (1 0 3) respectively. Apart from ZnO characteristic peaks, no phase corresponding to aluminum or other aluminum compounds was observed in the XRD patterns. This observation suggests that the films do not have any phase segregation or secondary phase formation as well as Al incorporation into ZnO lattice. The (0 0 2) peak appears with maximum intensity in pure and Al-doped films, which indicates that the preferred orientation of the crystals is the orientation with the c-axis perpendicular to the substrate. Thus, all the samples have strong preferred c-axis orientation. For films with high Al content (1.5% and 2% AZO films) the relative intensity of (1 0 0) and (1 0 1) peaks increases indicating some loss of the preferred c-axis orientation for heavily doped films.

Utilizing the XRD data, the average particle size was estimated from the Williamson–Hall (W–H) equation [34,35]

$$\beta \cos\theta = \frac{k\lambda}{D} + 4\varepsilon \sin\theta, \tag{1}$$

where λ is the wavelength of radiation used (1.5418 for CuK_α radiation used), k is the Scherrer constant, β is the full-width at half-maximum (FWHM) intensity of the diffraction peak for which the particle size is to be calculated, θ is the diffraction angle of the concerned diffraction peak, D is the crystallite dimension (or particle size) and ε is the microstrain. In general, the experimentally observed broadening (β_o) is the total contribution from particle size, strain broadening (β) and instrumental broadening (β_i). Thus, the broadening due to the size and strain (β) can be obtained from the experimentally observed broadening (β_o) using the equation [36]

$$\beta = \beta_\mathrm{o} - \beta_\mathrm{i}. \tag{2}$$

Diffraction data from standard silicon (Si) powder were used to measure the instrumental broadening [37,38]. The broadening (in FWHM) against 2θ obtained for standard silicon sample was plotted in a graph and was used as reference. The instrumental broadening at the observed peak positions for ZnO and Al-doped ZnO was evaluated from the graph.

X-ray line broadening analysis to evaluate FWHM (β) was carried out using the computer software (MARQ2) [39,40]. The software utilizes Marquardt least-squares procedure for minimizing the difference between the observed and simulated diffraction patterns. The peak shape and the intensity of reflection is modelled with a pseudo-Voigt (pV) analytical function, which is a combination of Gaussian and Lorentzian functions. The background intensity is subtracted by fitting the background with a suitable linear function. A typical plot of MARQ2 analysis for 0.5% AZO sample is shown in figure 2. The dotted curve represents the experimental intensity data (I_o) and the continuous curve represents the calculated (simulated) intensity data (I_c). The difference plot ($I_\mathrm{c} - I_\mathrm{o}$) is shown at the bottom.

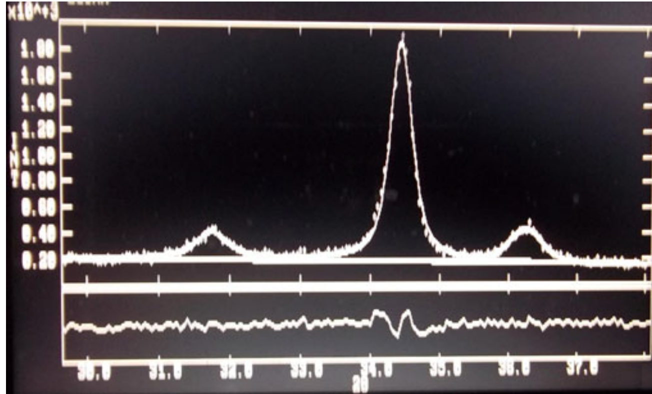

Figure 2. Observed (dotted) and simulated (continuous) X-ray diffraction patterns of 0.5% AZO.

From the values of β_o obtained using MARQ2 fitting and the corresponding values of instrumental broadening β_i, FWHMβ was calculated using eq. (2). Figure 3 shows the plot of $\beta\cos\theta$ vs. $4\sin\theta$ (W–H plots). The slope of the plots represents average

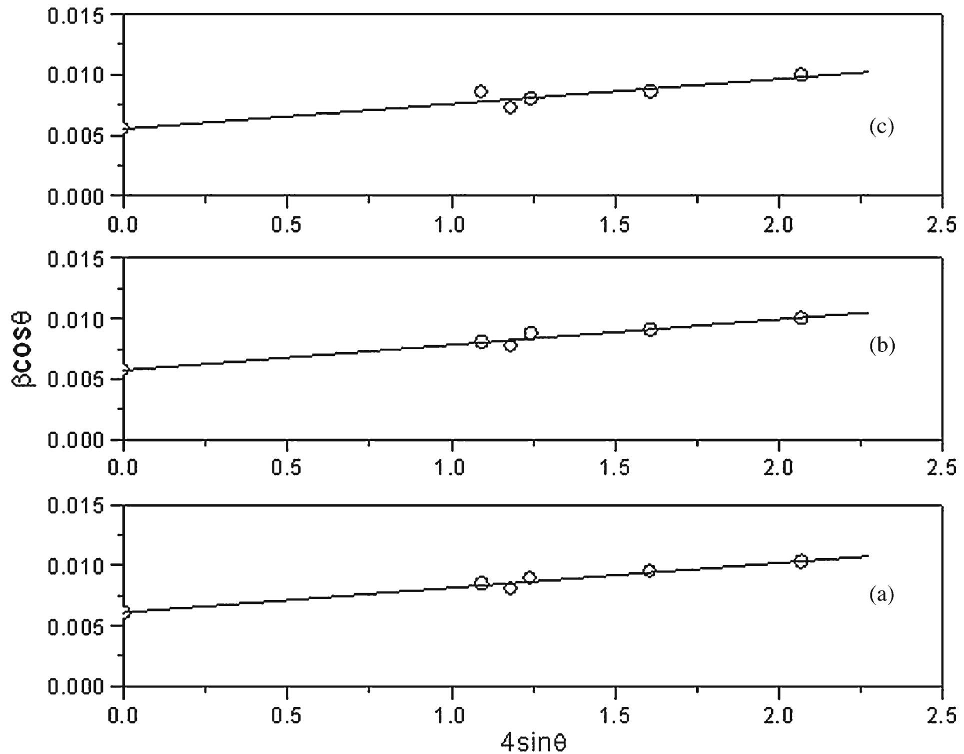

Figure 3. Williamson–Hall plots of (**a**) pure ZnO, (**b**) 1% Al:ZnO and (**c**) 2% Al:ZnO.

strain in the films whereas the inverse of intercept on $\beta \cos\theta$ axis gives the crystallite size (D) according to eq. (1). The particle size was evaluated using $k = 0.9$, which corresponds to spherical crystallites and $\lambda = 1.5418$, the wavelength of CuK_α radiation. The average value of particle size for pure ZnO is 22.75 nm. It increases to 24.26 nm for 1% Al:ZnO and to 25.13 nm for 2% Al:ZnO. Thus, with increasing doping concentration the particle size shows a slightly increasing trend. While a majority of the researchers have reported a marginal decrease in grain size due to Al incorporation [2,42,43], Rakhshani [27] has reported that Al-doping does not modify the size of the grains. In all these works Scherrer equation was applied to evaluate the grain size which only takes account of particle size broadening. In our present work we have utilized the W–H equation which is more accurate since it takes account of instrumental broadening and strain broadening also and accordingly gives much more reliable results compared to Scherrer equation. Such an increase in particle size may be due to the enhanced thickness of Al-doped films observed in our present work. It seems that the film tends to lower its surface energy as it becomes thicker during deposition. During the process, the lower surface energy grains may become larger as film thickness increases [44,45]. This is achieved by diffusion within a thin surface layer of atoms from a particular crystallite to one having a lower surface energy.

Figure 4 shows the SEM micrograph of pure and 1% AZO films. SEM image at normal incidence shows the microstructure of ZnO consisting of many spherical shaped crystalline particles. The grains more or less cover the substrate surface uniformly. However, AZO film shows particles with off-spherical shape. Thus, Al doping seems to have modified the shape of the grains. The microstructure is found to be uniform with compact interconnected grains. Also the film appears to have less porosity than pure ZnO film indicating that the film became denser with Al incorporation. Although no compositional analysis was attempted in the present study, the incorporation of Al in the films was verified by the EDAX result. Figure 5 shows the energy-dispersive X-ray spectrum of 0.5% Al:ZnO film. The spectrum reveals the presence of Zn, O and Al elements in the deposited films. The silicon signal appears from the substrate. Trace amounts of C and S impurities were also detected in the film.

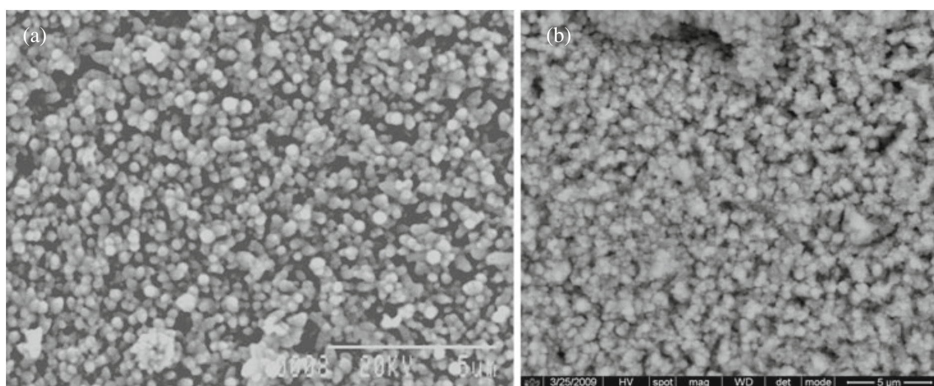

Figure 4. SEM image of (**a**) pure ZnO and (**b**) 1% Al:ZnO thin film.

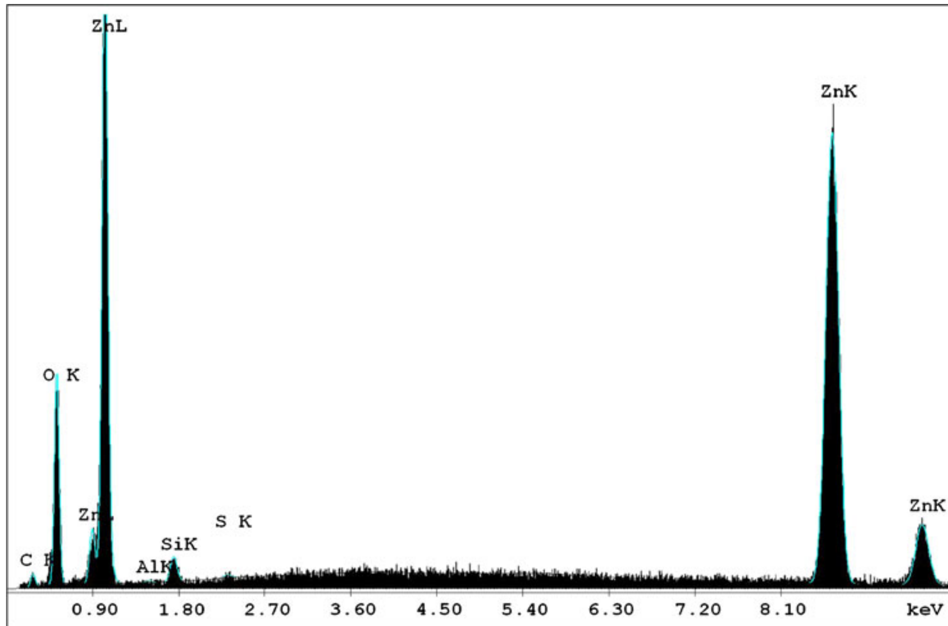

Figure 5. EDX pattern of 0.5% Al:ZnO.

3.2 *Optical absorption*

The optical absorbance spectrum measured within the wavelength range of 500–800 nm using a Shimadzu Spectrophotometer-1800 is shown in figure 6. The presence of a single

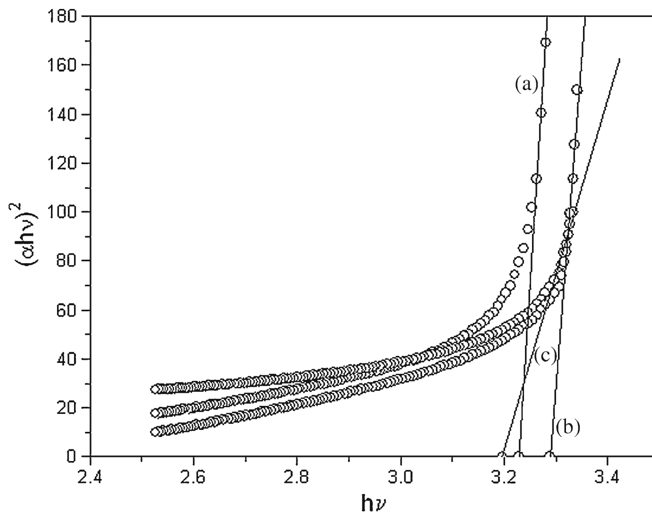

Figure 6. Plot of $(\alpha h\nu)^2$ vs. photon energy (in eV) of (**a**) pure ZnO, (**b**) 1% Al:ZnO and (**c**) 2% Al:ZnO.

slope in the plot suggests that the films have direct and allowed transition. It is also well known that ZnO is a direct band-gap material [41] and the energy gap (E_g) can thus be estimated by assuming direct transition between conduction band and valance bands. Theory of optical absorption gives the relationship between the absorption coefficients α and the photon energy $h\nu$ for direct allowed transition as

$$(\alpha h\nu)^2 = A(h\nu - E_g),$$

where A is a function of the index of refraction and hole/electron effective masses. The direct band gap is determined using this equation when linear portion of the $(\alpha h\nu)^2$ against $h\nu$ plot is extrapolated to intersect the energy axis at $\alpha = 0$. Plot of $(\alpha h\nu)^2$ against $h\nu$ for undoped and Al-doped ZnO films are shown in figure 6. Figure 6a shows the spectrum of pure ZnO while figures 6b and 6c shows the spectrum of 1% Al:ZnO and 2% Al:ZnO respectively.

The optical band gap shows an increase for 1% AZO compared to pure ZnO. For pure ZnO, the band gap is 3.228 eV and for 1% AZO, it increases to 3.29 eV. Such widening of optical band gap with aluminum doping is well described by Burstein–Moss effect [46–49]. For AZO films, compared to pure ZnO films, the contribution from Al^{3+} ions on substitutional sites of Zn^{2+} ions and Al interstitial atoms determines the widening of the band gap caused by increase in carrier concentration. This is the well-known Burstein–Moss effect and is due to the Fermi level moving into the conduction band. Since Al-doping increases the carrier concentration in the conduction band, the optical band-gap energy increases. Enhancement of band gap thus also ensures that aluminum was successfully doped in the ZnO thin films.

It is further observed in our present work that a decrease in band gap occurs for 2% AZO film. Such unusual red-shift of fundamental absorption edge has been reported by Mohanty *et al* [50] and has been explained in terms of stress relaxation mechanism. The reduction in slope of the linear portion of the plot (figure 6c) observed in our present work suggests introduction of defect states within the band gap. Thus we interpret this shift due to merging of an impurity band into the conduction band, thereby shrinking the band gap. Formation of such impurity band giving rise to new donor electronic states just below the conduction band is possible and this arises due to hybridization between states of the ZnO matrix and of the Al dopant [51]. It seems that such formation of donor levels compensates the Burstein–Moss effect and results in the narrowing of the effective band gap of AZO. The reduction of stress due to enhanced thickness [50] of AZO films compared to pure ZnO may also have some contribution to the observed red-shift.

3.3 *Electrical resistance*

The electrical resistance measurement of pure and Al-doped ZnO films were carried out in the surface mode using the conventional two-point probe technique. The resistance measurement was made in a Keithley 6514 system electrometer. The film was kept in the dark inside a tube furnace. Ohmic contacts using the conducting paste silver (curing temperature = 200°C) was made onto the surface of the film. Approximately 20 mm long silver (Ag) contacts, separated by 5 mm, were made on the films (30 mm × 25 mm) for electrical measurements. The width of the electrodes ∼1 mm. The electrical resistance was measured at 100°C. The films were heat treated at 200°C for 2 h prior to resistance

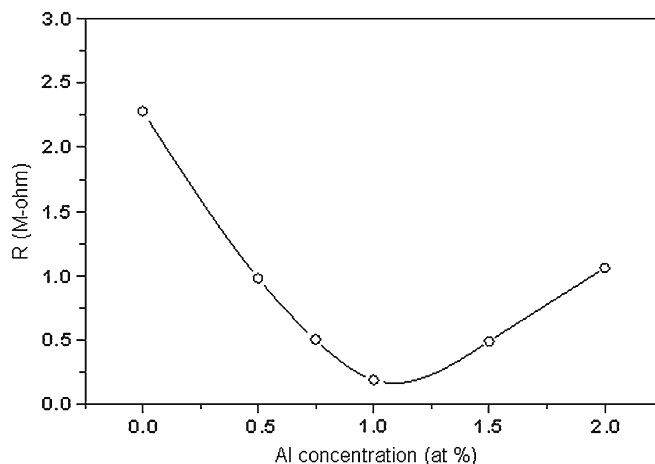

Figure 7. Variation of electrical resistance at 100°C with Al concentration.

measurements. It is seen from figure 7 that the resistance first decreases with increasing Al concentration and the lowest resistance is obtained at a doping concentration of 1 at %. With further increase in Al concentration the resistance value started to increase. The initial decrease of resistance with increase in Al concentration can be attributed to the increase in carrier concentration and also to the increase in mobility [16]. Beyond a certain doping concentration, a decrease in mobility but a small change in carrier concentration has been reported [21]. Our present observation suggests that beyond a certain doping concentration, the doping atoms do not occupy the lattice sites but instead result in some kind of defects. Such limited incorporation of Al into ZnO lattice is consistent with the results reported by researchers [16,52]. The defects produced beyond this optimum level of doping gives rise to states within the band gap reducing the effective band gap, which is observed in the present work. However, their contribution to the enhanced carrier density is neutralized by drastic decrease in mobility, thereby effectively reducing the resistance. Shrestha *et al* [42] reported this drastic reduction of mobility due to segregation of dopants at grain boundaries. It seems that the micro-mechanism of the influence of dopants is quite complicated. Thus, we can conclude that beyond certain doping concentration there is a segregation of dopant atoms at the noncrystalline regions which produces disorder in the lattice. These defects act as scattering centres giving rise to various scattering mechanisms resulting in a sharp decrease in mobility.

4. Conclusions

Undoped and Al-doped ZnO thin film could be successfully synthesized by the simple chemical technique SILAR. The films had good adherence to the substrate. Apart from being an inexpensive and simple technique, the method uses milder reaction conditions than those employed by most chemical methods proposed in the literature. XRD spectra show that the films are of hexagonal structure. Particle size evaluated using X-ray line broadening analysis and Williamson–Hall method shows a slightly increasing trend with

increasing Al incorporation. The average particle size for pure ZnO is 22.75 nm. It increases to 24.26 nm for 1% AZO film and 25.13 nm for 2% AZO film. Incorporation of Al was confirmed from elemental analysis using EDX. SEM micrograph shows spherical shaped particles for pure ZnO. Al doping seems to influence both the size and the shape of the grains. AZO films also appear to have a denser surface compared to pure ZnO. The band gap of the film increases upto a certain level of doping due to the increase of carrier density. Beyond this limit, there is a narrowing of band gap possibly indicating merging of an impurity band into the conduction band. The electrical resistance also decreases initially due to replacement of Zn ion by Al ions. Beyond a certain level of doping, the electrical resistance increases due to drastic fall in mobility arising out of segregation of dopants at grain boundaries.

Acknowledgements

One of the authors (PM) gratefully acknowledges CSIR (Council of Scientific and Industrial Research), New Delhi, India, for providing some financial support in the form of a research project [No. 03 (1195)/11/EMR-II].

References

[1] M Nirmala and A Anukaliani, *Photon. Lett. Poland* **2**, 189 (2010)
[2] S Tewari and A Bhattacharjee, *Pramana – J. Phys.* **76**, 153 (2011)
[3] K H Kim, R A Wibowo and B Munir, *Mater. Lett.* **60**, 1931 (2006)
[4] K Elmer, *J. Phys. D: Appl. Phys.* **33**, R17 (2000)
[5] K Arshak and I Gaiden, *Mater. Sci. Eng.* **B118**, 44 (2005)
[6] R Ghosh, S Fujihara and D Basak, *J. Electron. Mater.* **35**, 1728 (2006)
[7] C Ronning, P X Gao, Y Ding, Z L Wang and D Schwen, *Appl. Phys. Lett.* **84**, 783 (2004)
[8] L Yan, C K Ong and X S Rao, *J. Appl. Phys.* **96**, 508 (2004)
[9] F Paraguay, D M Miki-Yoshida, J Morales, J Solis and W Estrada, *Thin Solid Films* **373**, 137 (2000)
[10] B Baruwati, D K Kumar and S V Manorama, *Sens. Actuators* **B119**, 676 (2006)
[11] K V Gurav, V J Fulari, U M Patil, C D Lokhande and O Joo, *Appl. Surf. Sci.* **256**, 2680 (2010)
[12] S H Jeong, B N Park, D G Yoo and J H Boo, *J. Korean Phys. Soc.* **50**, 622 (2007)
[13] J Nishino, S Ohshio and K Kamata, *J. Am. Ceram. Soc.* **75**, 3469 (1992)
[14] J H Lee and B O Park, *Mater. Sci. Eng.* **B106**, 242 (2004)
[15] F K Shan, S Y Kim and Y S Yu, *Plasma Sci.* **2**, 312 (2003)
[16] J Mass, P Bhattacharya and R S Katiyar, *Mater. Sci. Eng.* **B103**, 9 (2003)
[17] K Yim and C Lee, *Crystal Res. Technol.* **41**, 1198 (2008)
[18] M Suchea, S Christoulakis, N Katsarakis, T Kitsopoulos and G Kiriakidis, *Thin Solid Films* **515**, 6562 (2007)
[19] Y E Lee, Y J Kim and H J Kim, *J. Mater. Res.* **13**, 1260 (1998)
[20] K Yamaya, Y Yamaki, H Nakanishi and S Chichibu, *Appl. Phys. Lett.* **72**, 235 (1998)
[21] D Raviendra and J K Sharma, *J. Appl. Phys.* **58**, 838 (1985)
[22] H M Zhou, D Yi, Z Yu, L Xiao and J Li, *Thin Solid Films* **515**, 6909 (2007)
[23] M Ohyama, H Kozuka and T Yoko, *J. Am. Ceram. Soc.* **81**, 1622 (1998)
[24] V Srikant, V Sergo and R Clarke, *J. Am. Ceram. Soc.* **78**, 1931 (1995)
[25] A V Singh, M Kumar, R M Mehra, A Wakahara and A Yoshida, *J. Ind. Inst. Sci.* **8**, 527 (2001)
[26] H Sato, T Minami, S Takata, T Miyata and M Ishii, *Thin Solid Films* **236**, 14 (1993)

[27] A E Rakhshani, *Appl. Phys.* **A92**, 413 (2008)
[28] S Mondal, K P Kanta and P Mitra, *J. Phys. Sci.* **12**, 221 (2008)
[29] P Mitra, *Mater. Sci. Res. India* **8**, 197 (2011)
[30] P Mitra and J Khan, *Mater. Chem. Phys.* **98**, 279 (2006)
[31] S Mondal and P Mitra, *Bull. Mater. Sci.* **35**, 751 (2012)
[32] S S Kale, R S Mane, H M Pathan, A V Shaikh, O S Joo and S H Han, *Appl. Surf. Sci.* **253**, 4335 (2007)
[33] Joint Committee on Powder Diffraction Standards, Inorganic Vol., B Post, S Weissmann and H F McMurdie (eds.), Card No. 36-1451, International Centre for Diffraction Data, Swarthmore, PA (1990)
[34] T Ungar and A Borbely, *Appl. Phys. Lett.* **69**, 3173 (1996)
[35] N Choudhury and B K Sarma, *Bull. Mater. Sci.* **32**, 43 (2009)
[36] H P Klug and L E Alexander, *X-ray diffraction procedures for polycrystalline and amorphous materials* (Wiley, New York, 1974)
[37] S Patra, P Mitra and S K Pradhan, *Mater. Res.* **14**, 17 (2011)
[38] P Sharma, A Gupta, K V Rao, F J Owens, R Sharma, R Ahuja, J M O Gullen, B Johansson and G A Gehring, *Nature Mater.* **2**, 673 (2003)
[39] X Jumin and J Wang, *Mater. Lett.* **49**, 318 (2001)
[40] B Ghosh, H Dutta and S K Pradhan, *J. Alloys and Compounds* **479**, 193 (2009)
[41] N Choudhury and B K Sarma, *Bull. Mater. Sci.* **32**, 43 (2009)
[42] S P Shrestha, R Ghimire, J J Nakarmi, Young Sung Kim, S Shrestha, C Y Park and J H Boo, *Bull. Korean Chem. Soc.* **31**, 112 (2010)
[43] O Lupan, S Shishiyanu, V Ursaki, H Khallaf, L Chow, T Shishiyanu, V Sontea, E Monaico and S Railean, *Solar Energy Materials and Solar Cells* **93**, 1417 (2009)
[44] J G E Gardeniers, Z M Rittersma and G J Burger, *J. Appl. Phys.* **83**, 7844 (1998)
[45] G Knuyt, C Quaeyhagens, J D'Haen and L M Stals, *Thin Solid Films* **258**, 159 (1995)
[46] E Burstein, *Phys. Rev.* **93**, 632 (1954)
[47] T S Moss, *Proc. Phys. Soc. London* **B67**, 775 (1954)
[48] B E Sernelius, K F Berggren, Z C Jin, I Hamberg and C Granqvist, *Phys. Rev.* **B37**, 10244 (1988)
[49] R Cebulla, R Wendt and K Ellmer, *J. Appl. Phys.* **83**, 1087 (1998)
[50] B C Mohanty, Y H Jo, D H Yeon, I J Choi and Y S Cho, *Appl. Phys. Lett.* **95**, 62103 (2009)
[51] S Gota, J R R Barrado, M Sanchez, N T Barrett, J Avila and M Sacchi, *Appl. Phys. Lett.* **86**, 042104 (2005)
[52] W Tang and D C Cameron, *Thin Solid Films* **238**, 83 (1994)